Advances in Military Technology
Vol. 21, No. 1, 2026, pp. 345-363
ISSN 1802-2308, eISSN 2533-4123
DOI 10.3849/aimt.02036

Passive Long-Wave Infrared Imaging for Ultra-Wide Temperature Applications

C. Toan Dang*, T. Baláž, and M. Kyselák

University of Defence, Brno, Czech Republic

The manuscript was received on 3 September 2025 and was accepted after revision for publication as an original research paper on 3 June 2026.

Abstract:

This paper presents a high-performance, fully passive athermalized long-wave infrared (LWIR) optical system for military and aerospace use. The design transitions from a paraxial framework to a realistic thick-lens configuration for high-fidelity optimization. The resulting system comprises only three lens elements and a single aspherical surface, achieving an aggressive aperture of f/1.2 and a 100 mm focal length. Rigorous evaluation via Zemax demonstrates that the design maintains near-diffraction-limited image quality and exceptional uniformity across an ultra-wide operational temperature range from −30 °C to 100 °C. By eliminating the need for active focusing mechanisms, this compact and lightweight solution offers superior reliability for long-range surveillance and aerial reconnaissance in extreme environments.

Keywords:

athermalized, optically athermalization, achromatic, triplet, athermal infrared lens

1 Introduction

Currently, contemporary thermal imaging systems typically operate within two primary atmospheric transmission windows: the mid-wave infrared (MWIR, 3–5 μm) and the long-wave infrared (LWIR, 8–14 μm). Owing to their robust performance in harsh environmental conditions such as fog, rain, and snow as well as their ability to operate in low-light or total darkness, these devices are extensively utilized across various sectors, including agriculture, industry, medicine, and defense [1–4].

A critical experimental characteristic of thermal imaging systems is the high sensitivity of image quality to fluctuations in ambient temperature. Infrared optical materials are limited in variety and are characterized by high coefficients of refractive index change according to temperature (dn/dT) and high coefficients of thermal expan-

* *Corresponding author: Department of Electrical Engineering, University of Defence, Brno, Kounicova 156/65, CZ-662 10 Brno, Czech Republic. Phone: +420 702 802 327, E-mail: dangchitoanchk28@gmail.com. ORCID 0009-0002-5763-5472.*

sion (CTE). The synergy of these factors often leads to thermal defocus, resulting in a severe degradation of system resolution. Consequently, in the optimal design of wide-temperature infrared optical systems, it is imperative to implement athermalization techniques to maintain focal plane stability, in addition to suppressing fundamental geometric aberrations.

Athermalization methods are generally categorized into three main approaches: active electromechanical, passive mechanical, and passive optical athermalization [2-4]. Active electromechanical methods utilize manual controls or servo motors to translate lens elements or mechanical components, thereby compensating for focal plane shifts induced by temperature variations [2]. Passive mechanical athermalization relies primarily on the integration of structural materials with disparate CTEs to automatically compensate for focal shifts. Meanwhile, passive optical athermalization focuses on selecting an optimal combination of optical materials based on the judicious correlation of their optical power, thermo-optic coefficients, and dispersion characteristics.

Although mechanical methods can be effective, they often require complex architectures, may consume additional power in active systems, and significantly increase the device's Size, Weight, and Power (SWaP) footprint. In contrast, passive optical athermalization facilitates a more compact and simplified structure by relying solely on the intrinsic physical properties of the materials and the strategic arrangement of the optical elements. However, this approach poses significant challenges due to the limited selection of infrared materials and the rigorous requirements for simultaneous aberration correction across broad spectral and temperature ranges. This necessitates extensive expertise in merit function optimization.

Regarding detector architecture, thermal imaging systems can be integrated with either cooled or uncooled detectors. Cooled detectors exhibit high thermal sensitivity within the MWIR band, making them superior for long-range target detection and identification; however, they are hindered by high costs and bulkiness due to the required cryogenic cooling units. Conversely, uncooled detectors, typically microbolometers, offer optimal sensitivity in the LWIR window and are suitable for targets with moderate thermal signatures, such as personnel or objects with temperatures close to the ambient environment. Due to their advantages in weight and compactness, uncooled systems are becoming increasingly prevalent. To compensate for their lower thermal sensitivity compared to cooled variants, the associated optical systems must feature large apertures (low *f*-number, typically $f/\# < 2$) to enhance photon collection efficiency.

Most previously published studies on passive athermalized LWIR optical designs have focused on systems with short focal lengths, small apertures, and narrow operating temperature ranges, which are primarily limited to civilian applications.

Aiming to optimize the device architecture, this paper proposes a design for an optically passively athermalized triplet lens system with a large aperture (low $f/\#$) operating in the LWIR spectrum, integrated with an uncooled detector. The system is engineered to maintain stable image quality across an ultra-wide operating temperature range through self-thermal compensation, meeting stringent standards for resolution, compactness, and operational stability required for military and airborne missions.

2 Basis of Optical System Calculation, Material and Main Parameters Selection

2.1 Calculations of Optical Systems

Expression for calculating the reciprocal relative dispersion of lens materials [5]:

$$v = \frac{n_{10} - 1}{n_8 - n_{12}} \tag{1}$$

where v is the reciprocal relative dispersion or Abbe number; n_8, n_{10}, n_{12} are the refractive indices of the optical material at wavelengths of 8 µm, 10 µm and 12 µm respectively. Formula of thermal-optical coefficient of lens material:

$$V = \frac{\beta}{n-1} - \alpha \tag{2}$$

where V is the thermal-optical coefficient; α is the coefficient of thermal expansion of the lens material (CTE); n is the refractive index; β is the thermal refractive index or the coefficient of refractive index change according to temperature (dn/dT).

For an ideal paraxial model, a change in temperature results in [5]:

$$\Delta n = \beta \Delta T \tag{3}$$

$$\Delta L = L\alpha\Delta T \tag{4}$$

$$\Delta f' = -f' V \Delta T \tag{5}$$

where Δn is the amount of change in refractive index of the lens material; ΔL is the amount of change in the dimensions of the lens such as thickness and radius of curvature; L is the dimensions of the lens such as thickness and radius of curvature; α is the coefficient of thermal expansion of the lens material (CTE); f' is the rear focal length of the lens; $\Delta f'$ is the change in rear focal length with temperature; ΔT is the temperature difference.

When the lens is in the housing, the change in the rear focal length of the lens with temperature is:

$$\Delta f' = -f'\left(V + \alpha_h\right)\Delta T \tag{6}$$

where α_h is the coefficient of thermal expansion of the housing.

Select the optical system to be designed consisting of 3 lenses. Use the following three equations to find the optical power of infinitely thin lenses.

Total optical power equation of the elements [6]:

$$\sum_{i=1}^{3} h_i \varphi_i = 1 \tag{7}$$

where φ_i is the optical power of the ith-lens; h_i is the height of incidence of the first-order auxiliary ray meeting each thin lens.

Condition to free chromatic aberration:

$$\sum_{i=1}^{3} \frac{h_i^2 \varphi_i}{v_i} = 0 \tag{8}$$

Athermalisation condition is given by:

$$\sum_{i=1}^{3} h_i^2 V_i \varphi_i = -\alpha_h \varphi \quad (9)$$

where V_i is the thermal-optical coefficient of the ith-lens; φ is the total optical power.

Materials used for the (8–12) µm spectral range are few compared to glass in the visible range, of which the most popular are Ge, ZnSe, ZnS. These three materials have the advantage of being stable in manufacturing technology and readily available on the market. Germanium has a high refractive index and low dispersion (see Tab. 1), so it is easy to eliminate chromatic and spherical aberration. However, its high thermal refractive index (β = 396) makes it difficult to eliminate thermal effect.

Tab. 1 Some common materials for LWIR band [7, 8]

Material	n @ $\lambda = 10$ µm	$\beta = \frac{dn}{dt}$ $[\times 10^{-6} K^{-1}]$	v	α CTE $[\times 10^{-6} K^{-1}]$	$V = \frac{\beta}{n-1} - \alpha$ $[\times 10^{-6} K^{-1}]$
Ge	4.003	396	750.75	5.7	126.168
ZnS	2.2	39	24	6.6	25.9
ZnSe	2.406	61	52.4626	7.1	36.285
IKS25	2.7675	46	152.370	22	4.025
Amtir1	2.4981	72	109.350	12	36.060
Amtir2	2.7691	30.7	162.302	22.4	−5.046
CdTe	2.649	50	164.9	4.5	25.821
GaAs	3.2786	185	105.004	5	76.190
Gasir-1	2.4944	55	119.552	17	19.804
KRS5	2.37069	−23.5	165.143	58	−75.144
NaCl	1.4947	−25	18.5977	44	−94.535
SchottIG6	2.7781	41	158.758	20.7	2.358

To achieve robust passive athermalization, the strategic selection of optical materials is paramount. This study utilizes a graphical selection method based on the thermal-optical map, where the triad of IKS25, ZnSe, and Germanium (Ge) was identified as an optimal combination. As illustrated in Fig. 1, the design space is defined by the Abbe number (v) on the horizontal axis and the product of the thermal-optical coefficient and the Abbe number ($V_i v$) on the vertical axis. Germanium acts as a critical vertex due to its extreme thermal-optical properties, positioning it far in the upper-right quadrant of the diagram. The significant lateral displacement between IKS25 and ZnSe establishes a broad baseline, resulting in a thermal-optical triangle with a substantial area. This large geometric area indicates a versatile solution space, allowing for the simultaneous correction of both chromatic and thermal aberrations while maintaining structural feasibility.

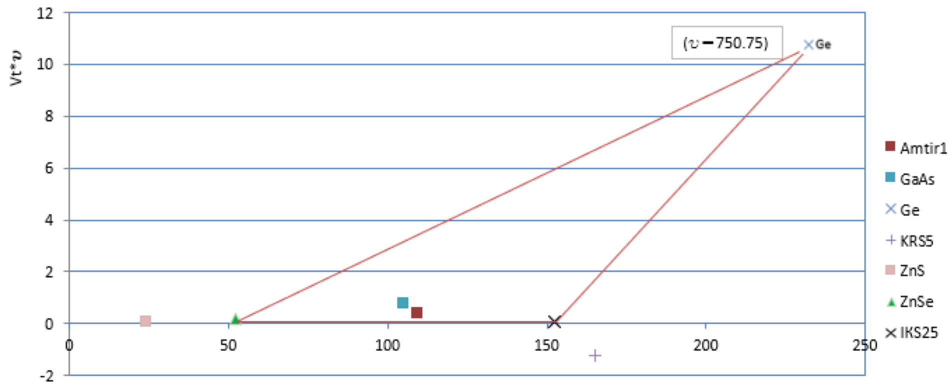

Fig. 1 LWIR band material distribution graph

2.2 Choose the Key Parameters of the Objective Lens

As noted in the introduction, this study adopts a simple and compact optical system design, therefore, the detector is uncooled. The detector must feature a sufficiently large focal plane array area and a sufficiently small pixel pitch to enhance target detection and recognition, while remaining compatible with a high-quality optical system design.

Depending on the air gap between the three lenses, choose invar with thermal expansion coefficient ($\alpha_h = 1.2 \times 10^{-6}$ K^{-1}) as the housing material [9]. Next, solve the system of Eqs (7)–(9) by numerical method to find the approximate solution as the optical powers of each optical element.

Other first-order and structural parameters, such as lens thicknesses and the clear apertures of each individual element, were determined and implemented using Zemax software.

The proposed LWIR optical system is designed with specific primary parameters to meet military requirements. These include the effective focal length (f'), the *f*-number (*f/#*), and the full field of view (2ω). The detailed specifications and target values for the design are summarized in Tab. 2:

Tab. 2 Main parameters of the objective lens

Detector size [μm × μm]	640 × 480
Pixel size [μm]	17
Working spectrum range [μm]	8–12
f' [mm]	100
2ω [°]	8
f/#	1.2
Optical system length [mm]	< 162
Back focal distant [mm]	> 13

 DOI 10.3849/aimt.02036

3 Results of LWIR Objective Design and Quality Analysis

In this work, a passively athermalized LWIR optical system is designed and optimized on the ZEMAX software. The optical system consists of a minimum of 3 lenses with three selected materials IKS25-ZnSe-Germanium. Initially, the IKS-25 material is imported as a Model into the Lens Data Editor (enter the refractive index and Abbe coefficient). The optical system is optimized for standard conditions of 20 °C and 1 atm pressure.

After achieving image quality, move on to changing the working temperatures in a relatively narrow range (from 10 °C to 50 °C). Using multiple configurations in ZEMAX, each configuration corresponds to a different temperature, while the pressure is kept constant. The optical layout of the athermalized triplet system is illustrated in Fig. 2.

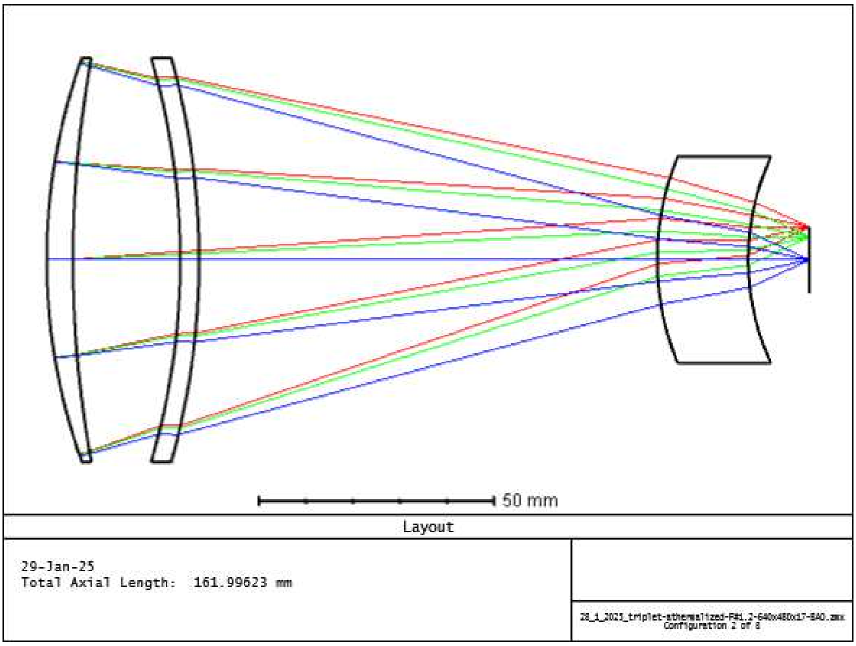

Fig. 2 Triplet objective optical system [10]

In the multi-configuration editor window, select Tools/Make thermal. Next, select Solve type as Thermal Pickup for the operands affected by temperature fluctuations including lens surface curvature (CRVT), thickness along the optical axis (THIC), lens half-diameter (SDIA). Note that a simple way to maintain nearly constant spacing between the three lenses is to use Invar, a material with a low coefficient of thermal expansion. Enter the thermal expansion coefficients of Invar and IKS25 into the TCEx1E-6 column at the bottom of the Lens data editor.

Optimize the optical system using the default Merit function: RMS – Spot Radius – Centroid. Run a Local Optimization first, then run Hammer Optimization [10].

The next step, extending the operating temperature range from −30 °C to 100 °C, necessitated the use of aspherical surfaces. This designed optical system uses only one aspherical surface on the rear surface of the first lens. The designed optical system data are given in Tabs 3 and 4.

Tab. 3 Parameters of optical system at 20 °C *(nominal)* [10]

N0	Radius	Thickness	Glass	Semi-Diameter	Conic
1	127.080	5.581	IKS25	43	
2	25.176	22.762		43	−0.995
3	−152.113	4	ZnSe	43	
4	−158.741	97.275		43	
5	57.434	19.329	Germanium	22	
6	52.185	13.053		22	
IMA	–	–		6.992	

Tab. 4 Aspheric coefficients of the second surface of the first lens

N0	2nd order term	4th order term	6th order term
2	−0.018	-1.818×10^{-8}	-6.539×10^{-13}

The Modulation Transfer Function (MTF) serves as the definitive metric for characterizing the imaging performance and contrast rendition of the proposed LWIR system. Spatial frequency is expressed in units of cycles per millimeter (cycles/mm). As illustrated in Fig. 3, the MTF of the optimized design closely approaches the theoretical diffraction limit, indicating a near-perfect correction of both monochromatic and chromatic aberrations. For a detector with a 17 μm pixel pitch, corresponding to a Nyquist frequency of approximately 29.4 cycles/mm, the system maintains an MTF value exceeding 0.5. This high contrast level at the critical spatial frequency demonstrates the superior sharpness and resolving power of the triplet configuration. Furthermore, the MTF curves exhibit remarkable stability and uniformity across the exhaustive ultra-wide thermal gradient from −30 °C to 100 °C. Such consistent performance confirms that the passive athermalization strategy effectively nullifies thermal defocusing, ensuring high-fidelity imaging for precision military and aerospace reconnaissance throughout extreme environmental transitions.

The imaging performance under thermal stress is rigorously evaluated through the MTF, which quantifies the ability of the system to transfer contrast from the object to the image plane. The contrast C_t at a specific spatial frequency v and temperature T is defined as:

$$C_t = \frac{I_{\max} - I_{\min}}{I_{\max} + I_{\min}}, \ 0 \le C_t \le 1$$

where I_{max} and I_{min} represent the maximum and minimum intensities of the imaged periodic structure, respectively.

To comprehensively evaluate the effectiveness of the passive athermalization strategy, the modulation transfer function variance, defined as $\Delta C = C_{20} - C_T$, was analyzed at three representative field angles: the on-axis field ($\omega = 0°$), the intermediate field ($\omega = 2°$), and the marginal field ($\omega = 4°$). The detailed results are presented in Figs 4–6.

DOI 10.3849/aimt.02036

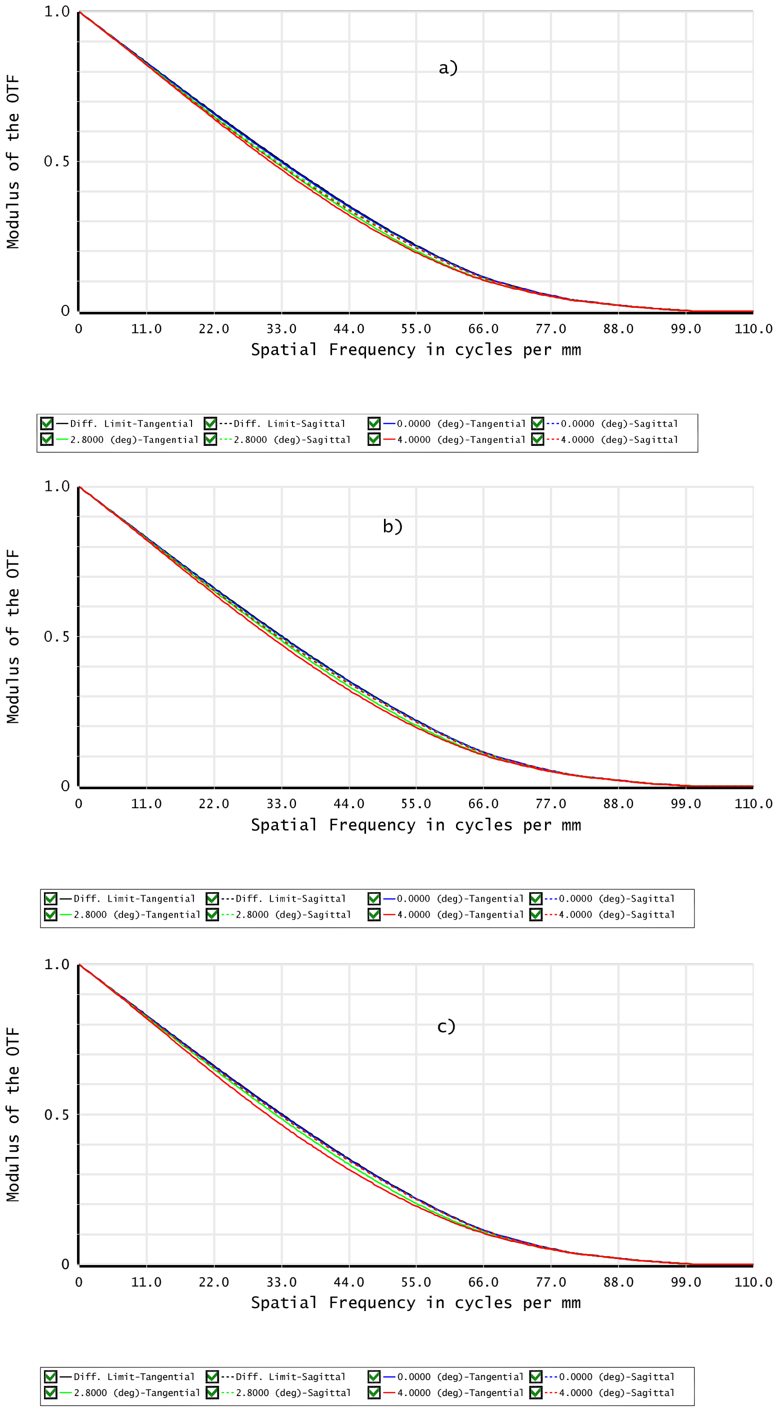

Fig. 3. a) MTF curve at 20 °C, *b) MTF curve at* –30 °C, *c) MTF curve at* 100 °C

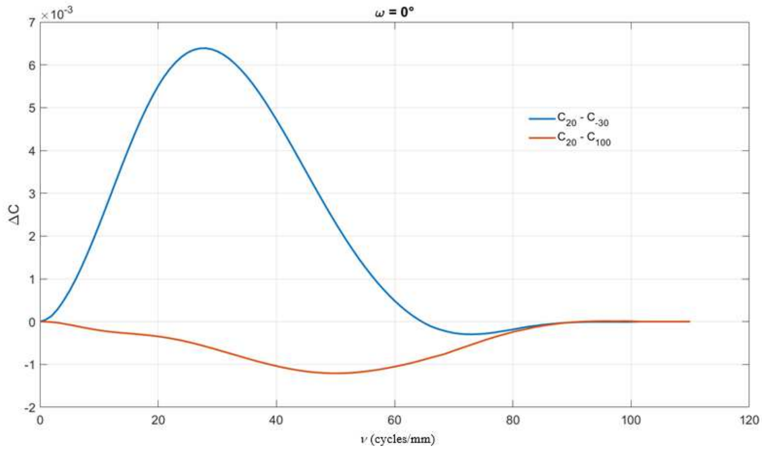

Fig. 4 Difference of MTF curves $\Delta C = C_{20} - C_{-30}$ *and* $\Delta C = C_{20} - C_{100}$ *of the designed lens for viewing angle* $\omega = 0°$

The most prominent observation from the data is the micro-scale amplitude of the MTF deviation ΔC. Throughout the extreme temperature range ($\Delta T = 130$ °C) and across spatial frequencies up to 110 cycles/mm, the absolute value of the variance remains consistently below 0.015. This confirms that the system maintains near-zero contrast degradation regardless of environmental fluctuations. At the center field ($\omega = 0°$), the maximum deviation is approximately 0.006 (Fig. 4). The intermediate field ($\omega = 2°$) exhibits even higher stability, with the variance strictly constrained within the range of 0 to −0.004 (Fig. 5). At the marginal field ($\omega = 4°$), despite a slight increase in variance due to the influence of off-axis high-order aberrations, the ΔC value remains optimally controlled at 0.014 (Fig. 6). The consistency of these results across the entire field of view demonstrates that the IKS25-ZnSe-Ge material triad successfully athermalizes the axial point while simultaneously maintaining a flat and stable focal plane.

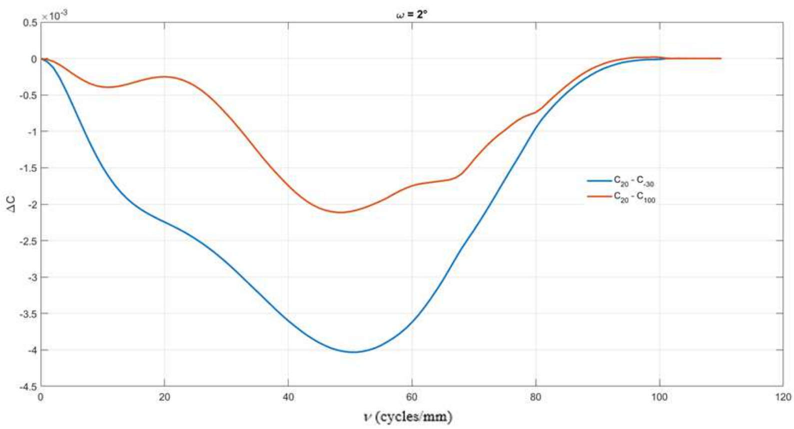

Fig. 5 Difference of MTF curves $\Delta C = C_{20} - C_{-30}$ *and* $\Delta C = C_{20} - C_{100}$ *of the designed lens for viewing angle* $\omega = 2°$

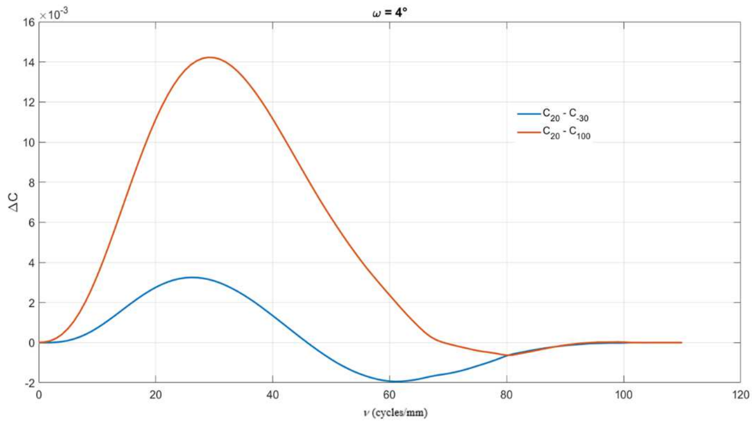

Fig. 6 Difference of MTF curves $\Delta C = C_{20} - C_{-30}$ *and* $\Delta C = C_{20} - C_{100}$ *of the designed lens for viewing angle* $\omega = 4°$

The most prominent observation from the data is the micro-scale amplitude of the MTF deviation ΔC. Throughout the extreme temperature range ($\Delta T = 130$ °C) and across spatial frequencies up to 110 cycles/mm, the absolute value of the variance remains consistently below 0.015. This confirms that the system maintains near-zero contrast degradation regardless of environmental fluctuations. At the center field ($\omega = 0°$), the maximum deviation is approximately 0.006 (Fig. 4). The intermediate field ($\omega = 2°$) exhibits even higher stability, with the variance strictly constrained within the range of 0 to –0.004 (Fig. 5). At the marginal field ($\omega = 4°$), despite a slight increase in variance due to the influence of off-axis high-order aberrations, the ΔC value remains optimally controlled at 0.014 (Fig. 6). The consistency of these results across the entire field of view demonstrates that the IKS25-ZnSe-Ge material triad successfully athermalizes the axial point while simultaneously maintaining a flat and stable focal plane.

To further evaluate the energy concentration and resolving power of the designed LWIR system, the spot diagrams across three representative temperatures are analyzed in Fig. 7. The black circle in each diagram represents the Airy disk, which defines the theoretical diffraction limit of the system with a radius of 14.65 μm.

At the standard operating temperature of 20 °C, the spot diagrams across all field angles (from 0° to 4°) are contained entirely within the Airy disk. The RMS radii at this temperature range from 1.41 μm to 3.42 μm, which are significantly smaller than the 14.65 μm Airy radius. This confirms that the system has achieved near-perfect aberration correction, reaching the theoretical diffraction limit.

Despite the significant temperature range of $\Delta T = 130$ °C, the spot size and shape remain remarkably stable at both –30 °C and 100 °C. At –30 °C, the RMS radii range from 1.485 μm to 3.033 μm. At 100 °C, the RMS radii are strictly controlled between 1.317 μm and 2.803 μm. The negligible variation in RMS radius across these extremes proves that the passive athermalization mechanism successfully prevents thermal defocusing as well as the emergence of significant high-order aberrations. The system exhibits consistent imaging quality from the center field to the marginal field of 4°. The minimal distortion of the spot shapes at the field edges indicates that off-axis aberrations, such as coma and astigmatism, have been effectively suppressed through the optimized use of aspherical surface and strategic material selection. Given a standard pixel pitch of 17 µm, the fact that the RMS radii remain below 4 µm ensures that the captured energy is concentrated primarily within a single pixel. This high level of concentration maximizes image sharpness and minimizes inter-pixel crosstalk, making the design ideal for high-resolution military and aerospace thermal imaging missions.

The energy concentration characteristics of the designed LWIR system were further evaluated using FFT Diffraction Encircled Energy (EE) plots, as shown in Fig. 8. These plots represent the fraction of total energy enclosed within a specific radius from the centroid of the image, providing a critical measure of contrast and sharpness for digital imaging sensors.

At the design reference temperature of 20 °C, the encircled energy curves for all field positions (0°, 2.8°, and 4°) almost perfectly overlap with the theoretical Diffraction Limit curve. Approximately 80 % of the energy is concentrated within a radius of 10 µm, and more than 90 % of the energy is contained within a 20 µm radius. This confirms that the triplet design achieves exceptional sharpness across the entire field of view. The stability of the energy concentration across the extreme temperature range is remarkable. The EE profiles at −30 °C and 100 °C remain virtually identical to the reference curves at 20 °C. There is no discernible degradation in energy concentration, proving that the passive athermalization strategy effectively maintains the focus and minimizes thermal aberrations over a total range of 130 °C.

The Point Spread Function (PSF) provides a direct visualization of the ability of the system to converge light from a point source, while the Strehl ratio serves as the most rigorous quantitative metric for evaluating imaging quality. Fig. 9 illustrates the Polychromatic Huygens PSF at the on-axis position (0°) for three temperature configurations to verify the efficacy of the passive athermalization mechanism.

An optical system is considered diffraction-limited when the Strehl ratio exceeds the 0.8 threshold [11]. The designed system significantly surpasses this benchmark with the following values. At the reference temperature of 20 °C, the Strehl ratio is 0.997. At the extreme cold of −30 °C, it remains exceptionally high at 0.974. At the extreme heat of 100 °C, it reaches 0.995. These results indicate that the system is essentially free of residual aberrations, preserving over 97 % of the peak intensity relative to an ideal, aberration-free system.

Observation of the 3D PSF structures in Fig. 9(a–c) reveals sharp, symmetric central peaks with negligible side lobes. This high energy concentration at the centroid ensures maximum image contrast and resolution, which is vital for detecting small thermal targets at long distances in military and aerospace applications.

The variation in the Strehl ratio across a wide thermal gradient of 130 °C is minimal, with a maximum deviation of only 0.023. This outcome confirms that the IKS25-ZnSe-Ge material triad successfully compensates for both thermal expansion and refractive index shifts (dn/dT). The system maintains absolute focal stability without requiring active mechanical or electronic refocusing mechanisms.

The chromatic focal shift is a critical metric for evaluating the ability of the system to focus multiple wavelengths onto a common image plane. Fig. 10 illustrates the chromatic focal shift across the 8–12 µm LWIR spectrum at an extreme operating temperature of −30 °C.

The simulation results reveal a Maximum Focal Shift Range of only 9.31 µm. When evaluated against the Diffraction Limited Range of 57.66 µm, the focal shift constitutes approximately only 16 % of the allowable depth-of-focus limit. This confirms that the chromatic shift is well-contained within the diffraction-limited bounds, ensuring that no significant chromatic defocusing occurs.

DOI 10.3849/aimt.02036

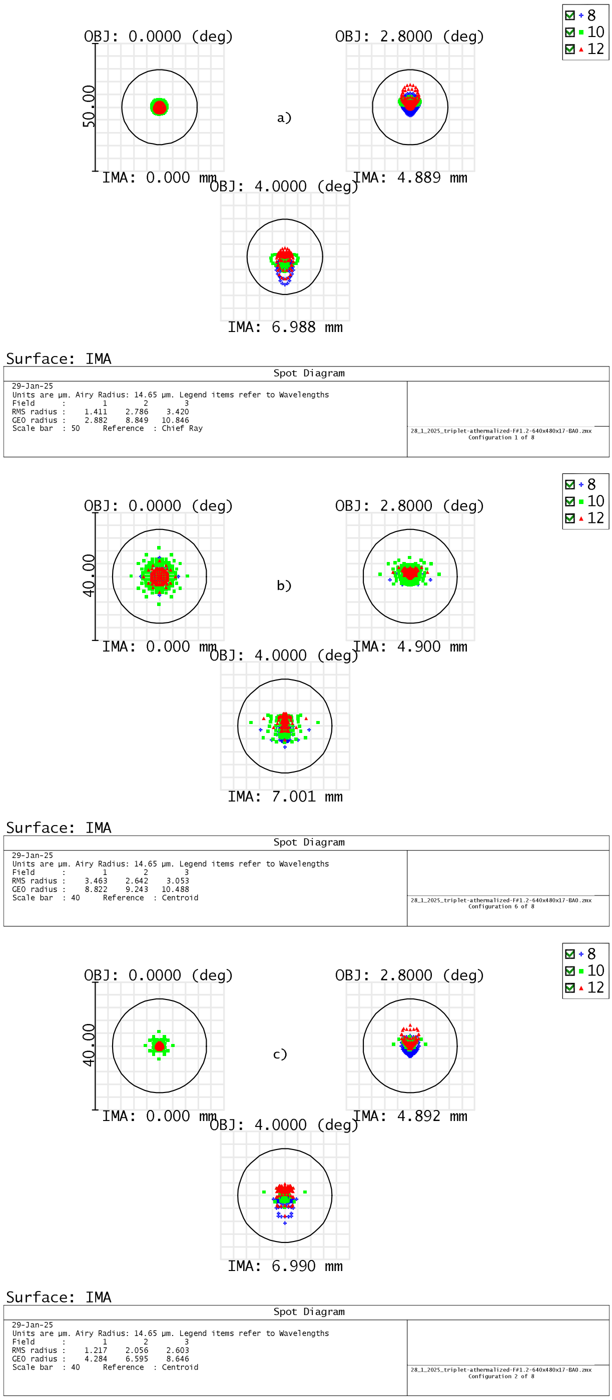

Fig. 7 a) Spot diagram at 20 °C, *b) Spot diagram at* −30 °C, *c) Spot diagram at* 100 °C

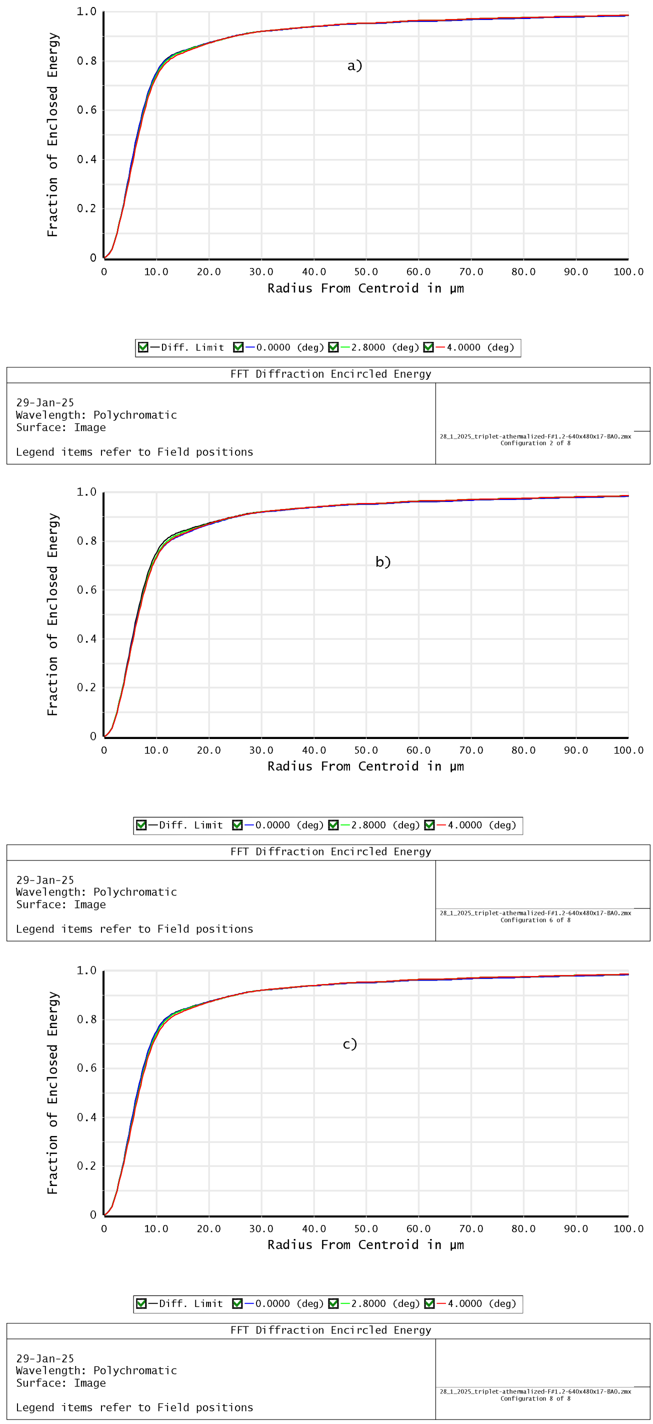

Fig. 8 a) Encircled energy at 20 °C, *b) Encircled energy at* −30 °C, *c) Encircled energy at* 100 °C

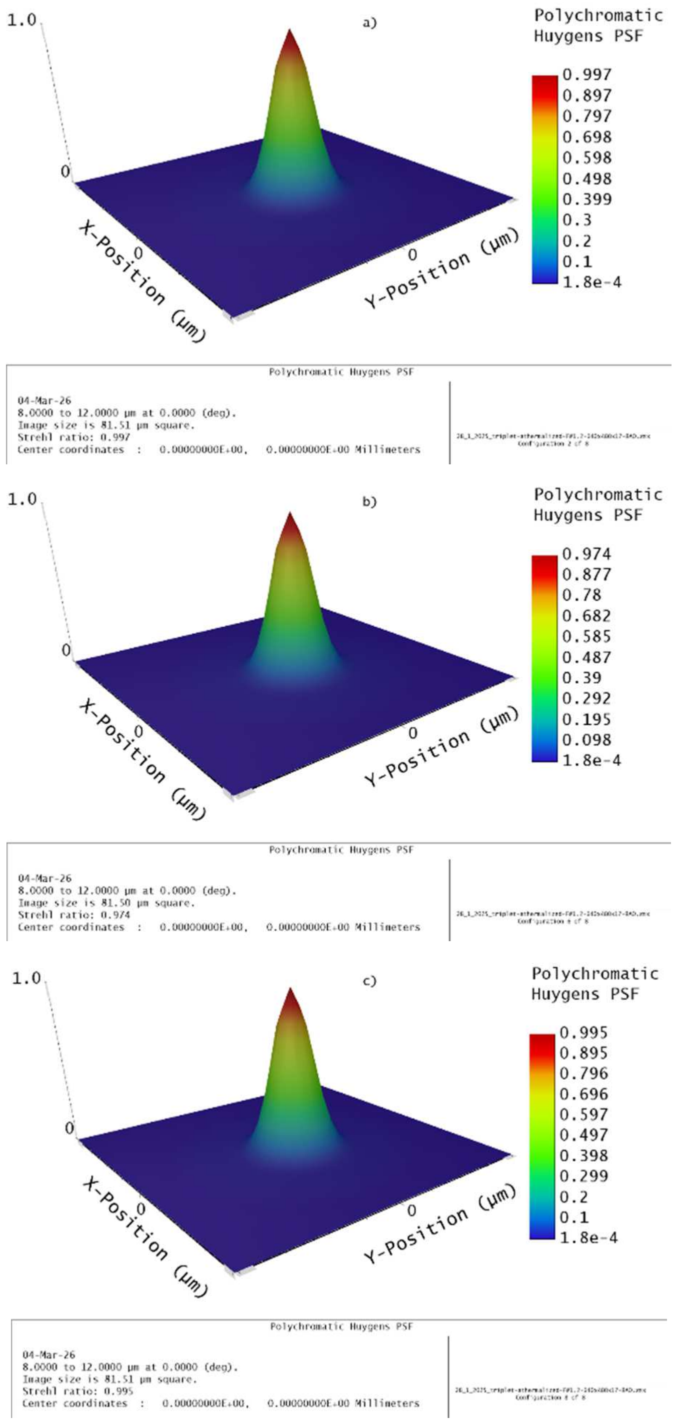

Fig. 9 a) On axis Strehl ratio at 20 °C*, b) On axis Strehl ratio at* −30 °C*, c) On axis Strehl ratio at* 100 °C

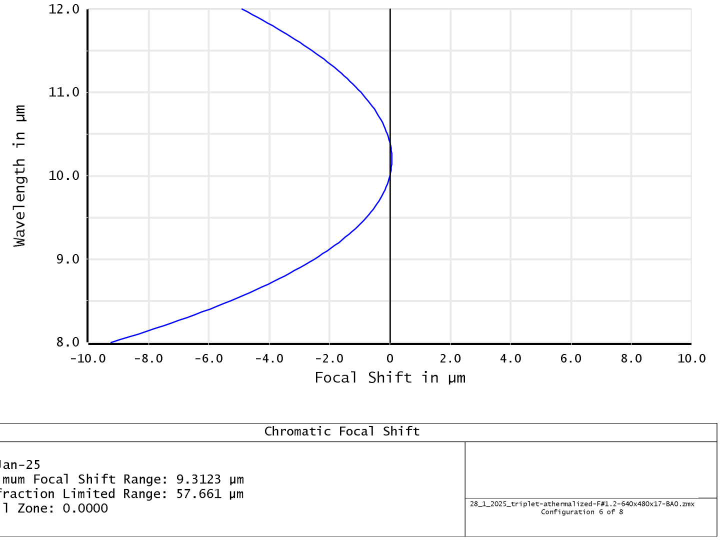

Fig. 10 Chromatic focal shift at −30 °C

The parabolic profile of the shift curve indicates that the dispersion characteristics of the IKS25-ZnSe-Ge triplet were precisely balanced to eliminate primary chromatic aberration. Efficiently controlling dispersion over a broad 4 µm spectral band is vital for maintaining high contrast in modern thermal imaging sensors.

By considering the image quality criteria mentioned above, it is clear that the designed optical system has significant advantages over the optical systems presented in the references [3, 12–14]. The system is highly simplified and has a long focal length, consisting of only three lenses, which enhances overall transmittance. It includes only one even aspheric surface, making manufacturing and testing feasible. Additionally, it uses two common optical materials and one chalcogenide material, all of which are commercially available.

The main drawback of the designed system is that the first lens is made of IKS25 material, which prevents the application of a diamond-like carbon (DLC) coating on the outermost surface [15]. To facilitate practical application, a thin protective window made of a widely available material, such as Germanium, can be placed in front of the system without degrading image quality.

4 Conclusions

This study successfully developed a high-performance LWIR objective lens featuring fully passive opto-mechanical athermalization and achromatization. Optimized for a 640 × 480 uncooled detector with a 17 µm pixel pitch, the system achieves a large focal length of 100 mm and a fast aperture of *f*/1.2. By utilizing a strategic IKS25-ZnSe-Ge material triad within a compact triplet architecture, the design maintains exceptional image quality across an ultra-wide operating temperature range from −30 °C to 100 °C.

The integration of a single even-order aspheric surface proved instrumental in expanding the thermal operational envelope while maintaining a simplified, three-lens structure. Comprehensive performance evaluations, including MTF stability analysis, spot diagrams, and Strehl ratio assessments, confirm that the system operates at the near-diffraction-limited threshold throughout the entire 130 °C thermal range. Specifically, the Strehl ratio remains above 0.97, and the chromatic focal shift is strictly controlled within 10 µm, representing only 16 % of the allowable diffraction-limited range.

These results demonstrate that the proposed design methodology effectively bridges the gap between analytical numerical modeling and high-precision manufacturing. The resulting optical system is fully mission-ready, offering a robust, lightweight, and thermally invariant solution for long-range surveillance, aerial reconnaissance, and target recognition in demanding military and aerospace environments.

Acknowledgements

This work was supported by the Ministry of the Interior of the Czech Republic – under grant VK01030060 – Instant Signal Processing Using Hybrid Systems in Defence Infrastructure and by the institutional support of the Ministry of Defence of the Czech Republic (SV24-217/1 and VAROPS).

References

[1] RIEDL, M.J. *Optical Design Fundamentals for Infrared Systems*. 2nd ed. Bellingham: SPIE Press, 2001. ISBN 0-8194-4051-5.

[2] JAMIESON, T.H. Thermal Effects in Optical Systems. *Optical Engineering*, 1981, **20**(2), pp. 156-160. DOI 10.1117/12.7972683.

[3] LI, H. and M. SHEN. An Optically Passive Athermal Infrared Optical System. In: *Proceedings of Current Developments in Lens Design and Optical Engineering IX*. San Diego: SPIE, 2008. DOI 10.1117/12.793649.

[4] SCHUSTER N. and J. FRANKS. Passive Athermalization of Two-Lens-Designs in 8-12 Micron Waveband. In: *Proceedings of Infrared Technology and Applications XXXVIII*. Baltimore: SPIE, 2012. DOI 10.1117/12.918112.

[5] SLYUSAREV, G.G. *Methods of Calculation of Optical Systems* (in Russian). 2nd ed. Leningrad: Mashinostroenie, 1969.

[6] GARSHIN, A.S. and G.I. TSUKANOVA. Structural and Design Features of Large Multispectral Optical Systems. *Journal of Optical Technology,* 2015, **82**(6), pp. 361-365. DOI 10.1364/JOT.82.000361.

[7] *Optical Materials* [online]. [viewed 2026-03-31]. Available from: https://www.crystran.co.uk/optical-materials

[8] AREFIEVA, K.I., et al. *Colored Optical Glass and Special Glasses. Catalog* (in Russian). Moscow: Dom Optiki, 1990.

[9] KREHEĽ, V., M. MOZOĽA, and M. KŘEPSKÝ. Materials and Technologies in the Design of Military Optical Devices. *Science & Military*, 2024, **19**(2), pp. 20-28. DOI 10.52651/sam.a.2024.2.20-28.

[10] *Ansys Zemax OpticStudio: Comprehensive Optical Design Software* [online]. [viewed 2025-06-09]. Available from: https://www.ansys.com/products/optics/ansys-zemax-opticstudio

[11] FISCHER, R.E., B. TADIC-GALEB and P.R. YODER. *Optical System Design*. 2nd ed. New York: McGraw Hill, 2008. ISBN 978-0-07-147248-7.

[12] ZHANG, Y., J.Y SHANG, Y. XU and W.S. WANG. Design of Cooled Athermalized Infrared Telephoto Lens. In: *Proceedings of Optical Design and Testing V*. Beijing: SPIE, 2012. DOI 10.1117/12.999327.

[13] SCHWERTZ, K., D. DILLON and S. SPARROLD. Graphically Selecting Optical Components and Housing Material for Color Correction and Passive Athermalization. In: *Proceedings of Current Developments in Lens Design and Optical Engineering XIII*. San Diego: SPIE, 2012. DOI 10.1117/12.930968.

[14] ROMANOVA, G.E. and G. PYŚ. Research of Aberration Properties and Passive Athermalization of Optical Systems for Infrared Region. In: *Proceedings of Optical Design and Engineering VI*. Jena: SPIE, 2015. DOI 10.1117/12.2191119.

[15] BELOUSOV, A.I. *Infrared Lens with Passive Thermalization*. Patent RU2629890C1 [online]. 2017 [viewed 2025-07-12]. Available from: https://patents.google.com/patent/RU2629890C1/en